JOURNAL OF GEOPHYSICAL RESEARCH, VOL. 111, D22211, doi:10.1029/2005JD006937, 2006

Past, present, and future concentrations of tropospheric ozone and aerosols: Methodology, ozone evaluation, and sensitivity to aerosol wet removal

Larry W. Horowitz[1]

Received 30 November 2005; revised 1 May 2006; accepted 16 June 2006; published 21 November 2006.

[1] Tropospheric ozone and aerosols are radiatively important trace species, whose concentrations have increased dramatically since preindustrial times and are projected to continue to change in the future. The evolution of ozone and aerosol concentrations from 1860 to 2100 is simulated on the basis of estimated historical emissions and four different future emission scenarios (Intergovernmental Panel on Climate Change Special Report on Emissions Scenarios A2, A1B, B1, and A1FI). The simulations suggest that the tropospheric burden of ozone has increased by 50% and sulfate and carbonaceous aerosol burdens have increased by factors of 3 and 6, respectively, since preindustrial times. Projected ozone changes over the next century range from −6% to +43%, depending on the emissions scenario. Sulfate concentrations are projected to increase for the next several decades but then to decrease by 2100 to 4–45% below their 2000 values. Simulated ozone concentrations agree well with present-day observations and recent trends. Preindustrial surface concentrations of ozone are shown to be sensitive to the assumed anthropogenic and biomass burning emissions, but in all cases they overestimate the few available measurements from that era. Simulated tropospheric burdens of aerosols are sensitive by up to a factor of 2 to assumptions about the rate of aerosol wet deposition in the model. The concentrations of ozone and aerosols produced by this study are provided as climate-forcing agents in the Geophysical Fluid Dynamics Laboratory coupled climate model to estimate their effects on climate. The aerosol distributions from this study and the resulting optical depths are evaluated in a companion paper by P. Ginoux et al. (2006).

Citation: Horowitz, L. W. (2006), Past, present, and future concentrations of tropospheric ozone and aerosols: Methodology, ozone evaluation, and sensitivity to aerosol wet removal, *J. Geophys. Res.*, *111*, D22211, doi:10.1029/2005JD006937.

1. Introduction

[2] Tropospheric concentrations of ozone and aerosols have increased considerably from preindustrial times as a result of anthropogenic emissions [e.g., *Volz and Kley*, 1988; *Staehelin et al.*, 2001]. Ozone and aerosols influence climate through their radiative forcings [e.g., *Ramaswamy et al.*, 2001] and are also major air pollutants affecting human health and vegetation [e.g., *World Health Organization*, 2003; *Mauzerall and Wang*, 2001]. Projected growth in anthropogenic emissions may increase concentrations of these species in the future, exacerbating their environmental impacts [*Prather et al.*, 2001]. This study considers the effect of changes in anthropogenic emissions on the concentrations of tropospheric ozone and aerosols during the period 1860–2100. Large emissions changes are estimated during this period [*Nakićenović et al.*, 2000; *van Aardenne et al.*, 2001] and are expected to dominate the change in ozone and aerosol concentrations [*Prather et al.*, 2001].

[3] The changes in ozone and aerosol abundances since preindustrial times are difficult to quantify because of sparse and uncertain preindustrial measurements, spatial heterogeneity in the distributions of these short-lived species, uncertain estimates of preindustrial emissions, and the nonlinear dependence of ozone on precursor emissions. Many recent studies have used chemical transport models to estimate the anthropogenic contribution to tropospheric ozone [*Berntsen et al.*, 1997; *Levy et al.*, 1997; *Wang and Jacob*, 1998; *Grenfell et al.*, 2001; *Hauglustaine and Brasseur*, 2001; *Mickley et al.*, 2001; *Shindell et al.*, 2003; *Lamarque et al.*, 2005] and aerosols [e.g., *Haywood and Boucher*, 2000; *Penner et al.*, 2001]. These studies typically suggest that anthropogenic activities have increased the burden of tropospheric ozone by 40–65%, but the actual change may be even larger [*Mickley et al.*, 2001]. The burdens of sulfate and carbonaceous aerosols are estimated to have increased by even more.

[4] Models have also been used in many recent studies to project future atmospheric concentrations of ozone and aerosols. These projections typically simulate a particular

[1]NOAA Geophysical Fluid Dynamics Laboratory, Princeton, New Jersey, USA.

target year (e.g., 2050, 2100) on the basis of available emissions scenarios, such as the 40 scenarios provided by the Intergovernmental Panel on Climate Change (IPCC) Special Report on Emissions Scenarios (SRES) [*Nakićenović et al.*, 2000]. In the IPCC Third Assessment Report (TAR), *Penner et al.* [2001] concluded that estimates of aerosol radiative forcing were highly uncertain, with the main sources of this uncertainty being aerosol emissions, wet removal, and optical properties. The OxComp study, conducted as part of the IPCC TAR, estimated that tropospheric ozone has increased by ~30% since the preindustrial period, and could increase by up to an additional 50% by 2100 [*Prather et al.*, 2001; *Gauss et al.*, 2003]. A more recent model intercomparison, conducted as part of the IPCC Fourth Assessment Report (AR4), estimated ±25% intermodel uncertainty in the predicted ozone change from 2000 to 2030, and demonstrated that air pollution controls could have significant effects on climate and nitrogen deposition, as well as air quality, over this time period [*Dentener et al.*, 2006; *Stevenson et al.*, 2006].

[5] This paper applies the global three-dimensional chemical transport model MOZART-2 [*Horowitz et al.*, 2003; *Tie et al.*, 2005] (*Horowitz et al.* [2003] are hereinafter referred to as H03) to estimate tropospheric ozone and aerosol (sulfate, black carbon, organic carbon, and mineral dust) concentrations from 1860 to 2100. The historical simulations (1860–1990) are based on the recently developed EDGAR-HYDE historical emissions inventory [*van Aardenne et al.*, 2001], while the future simulations (1990–2100) use emission projections from four different SRES scenarios (A2, A1B, B1, and A1FI) [*Nakićenović et al.*, 2000]. The simulations described here consider only the effects of emission changes, and neglect feedbacks from climate change and trends in stratospheric ozone.

[6] This study provides a consistent set of historical, present, and future concentrations of the short-lived radiative forcing agents, tropospheric ozone and aerosols, for use in climate studies. These ozone and aerosol distributions are used as inputs in the NOAA Geophysical Fluid Dynamics Laboratory (GFDL) coupled climate models CM2.0 and CM2.1 [*Delworth et al.*, 2006], in climate simulations for the IPCC AR4. These climate models simulate observed historical warming trends fairly realistically on the global scale and in many regions [*Knutsen et al.*, 2006]. In this paper, uncertainties in simulated ozone are assessed by comparison with observed concentrations. The aerosol concentrations are shown to be highly sensitive to the uncertain parameterization of wet removal. In a companion paper, we evaluate the aerosol concentrations simulated in this work, and the optical depths that are computed by CM2.1 using these aerosol fields, versus available ground-based and satellite observations [*Ginoux et al.*, 2006]. A future paper (V. Ramaswamy et al., manuscript in preparation, 2006) will present calculations of the radiative forcing caused by ozone and aerosols in CM2.1 climate simulations.

[7] The chemical transport model and emissions inventories used in this study are described in section 2. Model results for aerosol and ozone concentrations and burdens are presented in section 3. The simulated ozone concentrations are evaluated in section 4. Section 5 describes the sensitivity of model results to aerosol wet removal rates. Conclusions are presented in section 6.

2. Methodology

2.1. Model Setup

[8] The global chemical transport model Model for Ozone and Related Chemical Tracers, version 2.4 (MOZART-2), includes 63 gas-phase species as described by *H*03, 11 aerosol and precursor species to simulate sulfate and carbonaceous aerosols as described by *Tie et al.* [2005], and 5 size bins for mineral dust based on *Ginoux et al.* [2001]. The aerosol species simulated are sulfate, nitrate, ammonium, black carbon (BC: hydrophobic and hydrophilic), organic carbon (OC: hydrophobic, hydrophilic, and secondary organics), and mineral dust (5 diameter size bins, 0.2–2.0 μm, 2.0–3.6 μm, 3.6–6.0 μm, 6.0–12.0 μm, 12.0–20.0 μm). Hydrophobic black and organic carbon are chemically transformed into hydrophilic forms with a lifetime of 1.63 days [*Tie et al.*, 2005]. Following the approach used by *Tie et al.* [2005], different aerosol types are assumed to be externally mixed and do not interact with one another. Sulfur oxidation in the gas phase and within clouds is fully interactive with the gas-phase oxidant chemistry.

[9] The model is driven by meteorological inputs every three hours from the middle atmosphere version of the NCAR Community Climate Model (MACCM3) [*Kiehl et al.*, 1998]. The same meteorology is used for all simulations in this study. The horizontal resolution is 2.8° latitude × 2.8° longitude, with 34 hybrid sigma-pressure levels extending up to 4 hPa. The model time step for chemistry and transport is 20 min. MOZART is built on the framework of the Model of Atmospheric Transport and Chemistry (MATCH) [*Rasch et al.*, 1997], which rediagnoses convective mass fluxes using the *Hack* [1994] and *Zhang and McFarlane* [1995] schemes, and vertical diffusion within the boundary layer using the scheme of *Holtslag and Boville* [1993]. Tracer advection in MOZART is performed using a flux-form semi-Lagrangian scheme [*Lin and Rood*, 1996].

[10] Photolysis frequencies for clear-sky conditions are interpolated from a precalculated lookup table, on the basis of calculations using the Tropospheric Ultraviolet and Visible radiation model (TUV, version 3.0) [*Madronich and Flocke*, 1998]. The photolysis frequencies are modified to account for cloudiness [*Brasseur et al.*, 1998] but do not account for optical effects of the simulated aerosols. Heterogeneous hydrolysis of N_2O_5 and NO_3 on aerosol surfaces occurs at a rate based on the simulated sulfate surface area, with a reaction probability $\gamma = 0.04$ [*Tie et al.*, 2005]. Stratospheric concentrations of ozone and several other long-lived gases are constrained by relaxation to climatological values, as described by H03. Trends in stratospheric ozone are not accounted for in this study; concentrations are relaxed toward the present-day climatology in all simulations.

[11] Dry deposition velocities for gas-phase species are calculated off-line using a resistance-in-series scheme [*Wesely*, 1989; *Hess et al.*, 2000]. Deposition velocities for aerosol species are prescribed as by *Tie et al.* [2005]. Wet removal of soluble species in and below clouds is

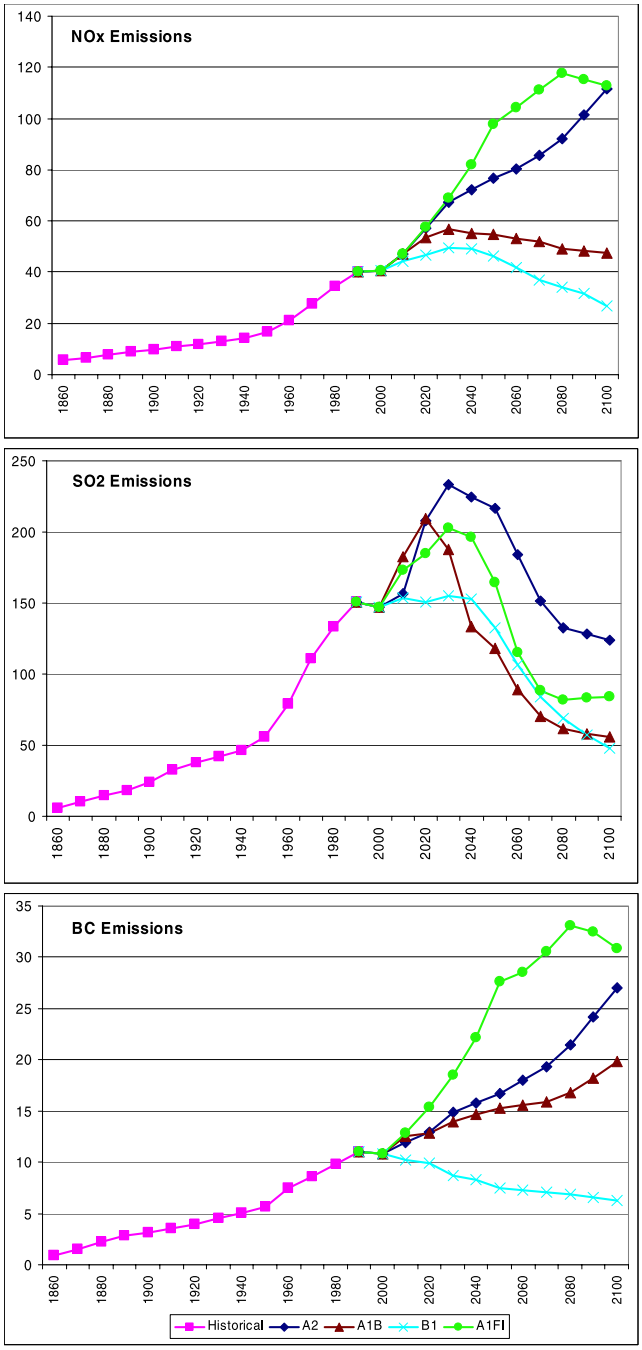

Figure 1. Global emissions of (top) NO_x (in Tg N yr^{-1}), (middle) SO_2, (Tg SO_2 yr^{-1}), and (bottom) black carbon (BC, Tg C yr^{-1}) for 1860–2100. See sections 2.2–2.4 for description of the emissions inventories. For the years 2010–2100, four different emissions scenarios are shown, based on the IPCC-SRES scenarios A2, A1B, B1, and A1FI. Emissions in 1990–2000 are identical in the four scenarios.

included as a first-order loss process, based on the large-scale and convective precipitation rates (H03). In-cloud scavenging is based on the parameterization of *Giorgi and Chameides* [1985], while below-cloud washout of highly soluble species follows *Brasseur et al.* [1998]. For gas-phase species, the removal rate depends strongly on the temperature-dependent effective Henry's law constant. Wet deposition of soluble aerosols (sulfate, hydrophilic BC, hydrophilic OC, ammonium, and nitrate) is calculated by scaling the removal rate to that of highly soluble HNO_3, assuming the aerosols have a first-order loss rate constant equal to 20% of that of HNO_3 [*Tie et al.*, 2005]. This scaling introduces a large uncertainty into the calculation of aerosol burdens. The sensitivity of model results to this scale factor is discussed below (section 5). Wet removal of dust is calculated using the formulation of *Zender et al.* [2003], with below-cloud scavenging efficiencies of 0.02 m^2 kg^{-1} for convective and 0.04 m^2 kg^{-1} for stratiform precipitation.

[12] This study focuses on the historical and future changes in ozone and aerosol concentrations driven by changes in anthropogenic emissions. Model emissions are described below in sections 2.2–2.4. Two-year MOZART simulations are performed as "snapshots" each decade from 1860 to 2100; the first year is used for spin-up and the second year is analyzed. Initial concentrations of tracers are specified on the basis of a previous MOZART simulation and are particularly important for methane because its atmospheric adjustment timescale exceeds the two-year length of the model simulations.

2.2. Present-Day Emissions

[13] Emissions of gas-phase species in 1990 are the same as those used by H03. Emissions from fossil fuel sources are from EDGAR v2.0 [*Olivier et al.*, 1996], except for BC and OC, which are based on *Cooke et al.* [1999] (organic carbon emissions were doubled from the Cooke et al. value to account for rapidly produced secondary organic aerosols, as suggested in that work). Biomass burning is based on *Hao and Liu* [1994] in the tropics and *Müller* [1992] in the extratropics, with emission ratios from *Andreae and Merlet* [2001]. The biomass burning inventory used is "climatological," and does not vary from year to year to reflect the actual burning occurring during specific years. BC is emitted as 80% hydrophobic and 20% hydrophilic, while OC is emitted as 50% hydrophobic and 50% hydrophilic [*Tie et al.*, 2005]. Biogenic emissions of isoprene and monoterpenes are from GEIA [*Guenther et al.*, 1995], with a 25% reduction in tropical isoprene emissions based on more recent evidence that they may be overestimated by GEIA (see H03). Soil NO_x is from *Yienger and Levy* [1995]. The source of NO_x from lightning is parameterized on the basis of convective cloud top heights [*Price et al.*, 1997] and is scaled to produce a total of 3 Tg N yr^{-1}. Aircraft emissions of NO_x and CO are based on *Friedl* [1997]. Emissions of SO_2 include 141 Tg yr^{-1} from anthropogenic activities, 4.5 Tg yr^{-1} from biomass burning, and 5.4 Tg yr^{-1} from volcanoes. The oceanic source of dimethyl sulfide (DMS) provides 15.5 Tg S yr^{-1}. Dust emissions were calculated interactively, on the basis of surface wind speed as described by *Ginoux et al.* [2001]. Natural sources, including dust, biogenic emissions, volcanoes, and oceans, are identical in all simulations conducted.

2.3. Historical Emissions

[14] Historical emissions from 1890 to 1980 are based on the EDGAR-HYDE v1.3 inventory [*van Aardenne et al.*, 2001], which includes anthropogenic emissions of CO_2, CO, CH_4, nonmethane volatile organic compounds

Table 1. Surface Emissions of NO_x, CO, Black Carbon, Organic Carbon, and SO_2 Used in Historical and Present-Day Simulations[a]

Year	NO_x, Tg N yr^{-1}	CO, Tg yr^{-1}	BC, Tg C yr^{-1}	OC, Tg C yr^{-1}	SO_2, Tg yr^{-1}
1860	5.5	306	0.9	9.3	5.8
1870	6.7	366	1.6	12.4	10.0
1880	7.8	427	2.2	15.6	14.2
1890	9.0	487	2.8	18.7	18.4
1900	9.8	516	3.1	20.2	24.1
1910	10.9	554	3.6	22.1	32.9
1920	11.9	592	4.0	24.1	37.3
1930	13.1	638	4.5	26.5	42.4
1940	14.2	676	5.0	28.5	46.2
1950	16.6	719	5.7	30.9	56.1
1960	21.2	848	7.5	37.3	79.1
1970	27.5	960	8.6	42.2	111.2
1980	34.5	1072	9.8	47.2	133.4
1990	40.3	1195	11.0	52.3	150.9

[a]As described in sections 2.2 and 2.3. BC, black carbon; OC, organic carbon.

(NMVOCs), SO_2, NO_x, N_2O, and NH_3. In order to avoid discontinuities between the EDGAR-HYDE historical emissions and the standard 1990 MOZART emissions (section 2.2 and H03), the EDGAR-HYDE emissions are scaled (for all years) such that the EDGAR-HYDE 1990 global totals for each species and source type match those in the MOZART 1990 emissions. This scaling allows the time variation in emissions from EDGAR-HYDE to be used, while maintaining present-day emissions consistent with H03, and allows for extension to the future (see section 2.4). Historical emission totals for NO_x, SO_2, and BC are shown in Figure 1 (details in Table 1).

[15] The EDGAR-HYDE inventory does not include emissions of BC or OC. Emissions of these species are estimated by scaling emissions to those of CO for each source type, since all three of these species are products of incomplete combustion. The geographic patterns of present-day emissions for BC and OC differ somewhat from those for CO, so the transition from present-day emission patterns to those based on scaling to historical CO emissions is introduced gradually from 1960 to 1980. Before 1960, BC and OC emissions are scaled to CO. Historical emissions from aircraft are estimated by assuming a growth rate of approximately 5% yr^{-1} from 1940 to 1990 (based on *Henderson and Wickrama* [1999]), with zero emissions before 1940. Because the atmospheric lifetime of methane is much greater than the two-year length of the model simulations, it is insufficient to change just the emissions of methane in MOZART. Initial concentrations of methane are scaled uniformly to match historical global-mean surface concentrations [*Prather et al.*, 2001].

[16] The time series of emissions are extended from 1890 (the earliest year included in EDGAR-HYDE) back to 1860 (intended here to represent "preindustrial" conditions) by setting fossil fuel burning to zero and setting soil NO_x emissions to preindustrial values (3.6 Tg N yr^{-1} [*Yienger and Levy*, 1995]). Emissions from burning of biofuels, savannah, tropical forests, and agricultural waste in 1860 are assumed to be 10% of 1990 values (a standard assumption, made by *Levy et al.* [1997], *Wang and Jacob* [1998], *Mickley et al.* [1999, 2001], *Grenfell et al.* [2001], and *Shindell et al.* [2003]). In the EDGAR-HYDE inventory, the 1890 global emissions of CO from these sources are reduced to 37% (biofuel), 30% (savannah), 31% (tropical forest fires), and 52% (agricultural waste burning) of their 1990 values. Extratropical forest burning, which is not included in EDGAR-HYDE, is assumed to be primarily natural and is maintained at constant values from 1860 to 1990. The sensitivity of results to this assumption is discussed below (sections 3.1 and 4.2). Emissions for 1870–1880 were estimated by linear interpolation between the 1860 (preindustrial) and 1890 values. This approach produced a consistent time series of emissions from 1860 to the present.

2.4. Future Emissions Scenarios

[17] Four potential future emission scenarios are considered in this study: the A2, A1B, B1, and A1FI scenarios developed for the IPCC SRES [*Nakićenović et al.*, 2000]. Version 1.1 of the SRES marker scenarios A2-ASF, A1B-AIM, B1-IMAGE, and A1G-MINICAM were downloaded from http://www.grida.no/climate/ipcc/emission/164.htm. Anthropogenic emissions of CH_4, N_2O, SO_x, CO, NMVOC, and NO_x in four geopolitical regions (OECD90, REF, ASIA, and ALM) were obtained from the SRES scenarios for each decade 1990–2100 (the scenarios all have identical emissions for 1990 and 2000). Future scenario emissions in MOZART were obtained by scaling the standard 1990 anthropogenic emissions (section 2.2) by the ratio of SRES emissions for each future decade to that for 1990 in each of the four regions. For the purpose of this scaling, all fossil fuel and biofuel emissions and 50% of the biomass burning emissions (both tropical and extratropical) were assumed to be anthropogenic. This assumption, which is different from that assumed for historical emissions (section 2.3), was made in order to allow MOZART "anthropogenic" emissions to reproduce approximately the SRES regional emission totals for 1990. The SRES scenarios do not include emissions of BC and OC. Future scenario emissions of these species were estimated by using the corresponding emission change ratios prescribed for CO, similar to the assumption made for historical emissions (section 2.3). Global emission totals of NO_x, SO_2, and BC in 1990–2100 for the four scenarios are shown in Figure 1 (details in Table 2). In addition to scaling emissions of methane, the initial conditions for methane were scaled to match the global average methane abundances specified in the appropriate SRES scenario.

3. Model Results

3.1. Historical Results (1860–2000)

[18] The tropospheric burden of ozone increases globally by 50% (10.81 DU, or 118.0 Tg) from preindustrial times (1860) to the present (2000), with more than half of this increase occurring since 1950 (Figures 2 and 3 and Table 3; tropospheric column is defined in the Figure 2 caption). This increase in tropospheric ozone burden is within the range calculated by other modeling studies of 71–140 Tg [*Lamarque et al.*, 2005, and references therein]. Industrial emissions of ozone precursors (most importantly NO_x) cause the chemical production of tropospheric ozone to increase by more than a factor of 2 (Table 4), driving large increases in ozone columns in the northern middle to high latitudes (+12–20 DU), while increased biomass

Table 2. Surface Emissions of NO_x, CO, Black Carbon, Organic Carbon, and SO_2 Used in Future Scenario Simulations[a]

	A2				A1B				B1				A1FI			
Year	NO_x, Tg N yr^{-1}	CO, Tg yr^{-1}	BC, Tg C yr^{-1}	OC, Tg C yr^{-1}	SO_2, Tg yr^{-1}	NO_x, Tg N yr^{-1}	CO, Tg yr^{-1}	BC, Tg C yr^{-1}	OC, Tg C yr^{-1}	SO_2, Tg yr^{-1}	NO_x, Tg N yr^{-1}	CO, Tg yr^{-1}	BC, Tg C yr^{-1}	OC, Tg C yr^{-1}	NO_x, Tg N yr^{-1}	CO, Tg yr^{-1}	BC, Tg C yr^{-1}	OC, Tg C yr^{-1}	SO_2, Tg yr^{-1}
2000	40.5	1195	10.9	51.5	147	40.5	1195	10.9	51.5	147	40.5	1195	10.9	51.5	40.5	1195	10.9	51.5	147
2010	47.2	1284	12.0	55.6	157	47.0	1317	12.5	57.1	183	44.2	1131	10.2	48.3	47.2	1334	12.8	58.3	173
2020	57.4	1369	13.0	59.5	208	53.5	1343	12.8	58.1	209	46.8	1100	9.9	46.9	57.5	1506	15.3	67.0	185
2030	67.4	1526	14.9	67.1	233	56.9	1422	14.0	61.9	187	49.4	984	8.7	41.8	69.1	1718	18.6	78.9	203
2040	72.1	1596	15.8	70.7	225	55.0	1469	14.6	64.1	134	49.2	929	8.2	39.5	82.1	1977	22.1	92.3	196
2050	76.6	1667	16.7	74.4	216	54.9	1520	15.3	66.5	118	46.3	872	7.5	36.8	97.8	2376	27.7	112.2	164
2060	80.3	1769	18.0	79.5	184	53.0	1546	15.6	67.6	89	41.7	858	7.2	36.2	104.4	2469	28.6	115.8	115
2070	85.7	1872	19.4	84.6	151	52.0	1573	15.9	68.9	70	37.0	853	7.1	35.9	111.0	2644	30.5	123.8	88
2080	92.3	2030	21.4	92.3	133	49.3	1642	16.8	72.1	61	34.2	829	6.9	34.8	117.8	2889	33.0	134.0	82
2090	101.5	2245	24.2	102.8	128	48.3	1764	18.2	77.8	58	31.5	806	6.6	33.7	115.4	2825	32.5	130.8	83
2100	111.7	2458	27.0	113.2	124	47.4	1904	19.9	84.3	56	26.9	777	6.3	32.3	112.7	2724	30.9	124.7	84

[a]See section 2.4 for details. BC, black carbon; OC, organic carbon.

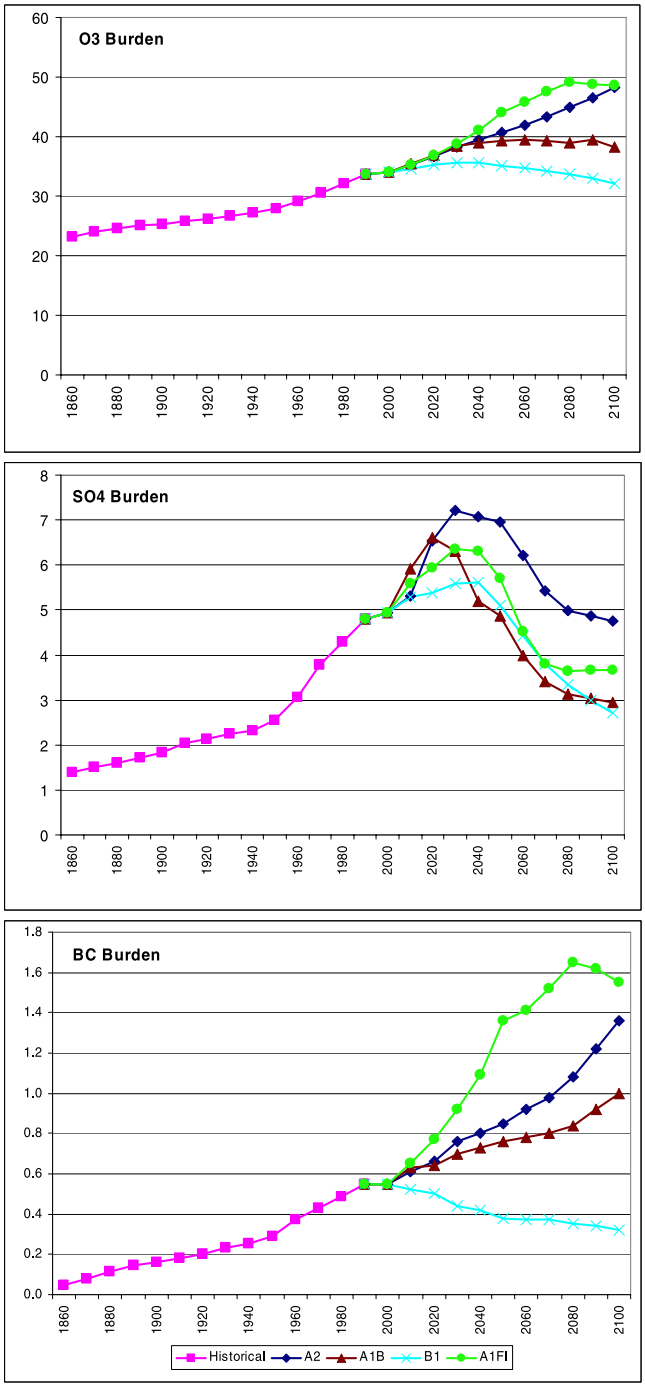

Figure 2. Simulated global average burdens of (top) tropospheric ozone (in Dobson units, 1 DU = 2.687 × 10^{16} molecules/cm^2), (middle) total sulfate aerosol (mg $SO_4^{=}/m^2$), and (bottom) total black carbon aerosol (BC, mg C/m^2) for 1860–2100. For the years 2010–2100, results are shown for simulations using emissions based on the IPCC-SRES scenarios A2, A1B, B1, and A1FI. The tropospheric column is calculated as the sum from the surface to the "chemical tropopause," defined as the lowest model level with monthly mean O_3 mixing ratio exceeding 150 ppbv (in the 1990 base case simulation) [*Prather et al.*, 2001].

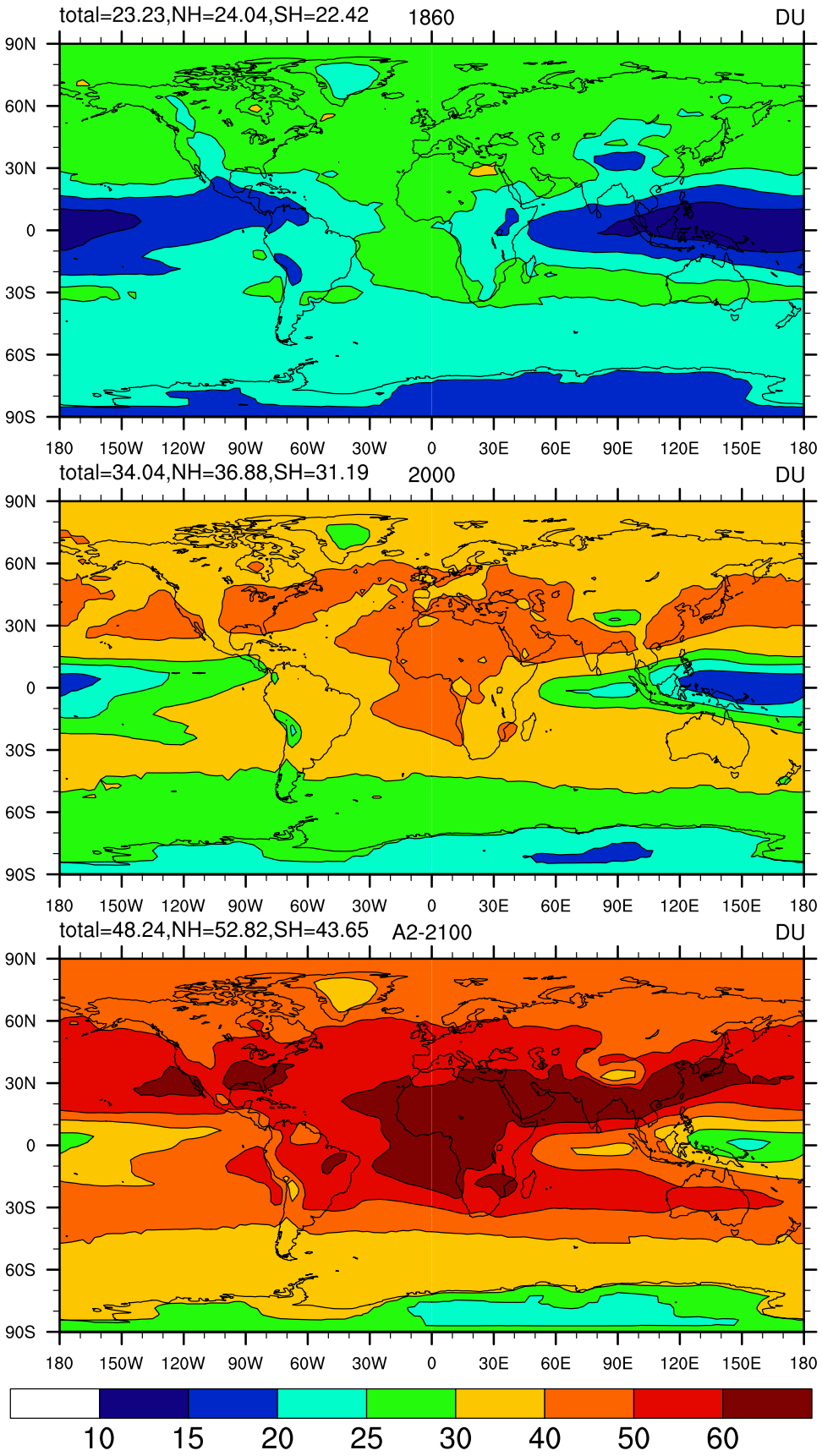

Figure 3. Total tropospheric column of ozone (in DU) in simulations for (top) 1860 and (middle) 2000 and (bottom) the A2 scenario for 2100. The tropospheric column is calculated as in Figure 2.

Table 3. Global Burdens of Ozone, Black Carbon, Organic Carbon, and Sulfate From Historical and Present-Day Simulations[a]

Year	O_3	BC	OC	$SO_4^=$
1860	253.6	0.03	0.21	0.70
1870	262.5	0.04	0.30	0.77
1880	268.0	0.06	0.38	0.82
1890	273.0	0.08	0.46	0.87
1900	276.5	0.08	0.50	0.94
1910	281.2	0.09	0.55	1.04
1920	286.1	0.10	0.60	1.09
1930	291.4	0.12	0.66	1.14
1940	296.8	0.13	0.71	1.19
1950	303.7	0.15	0.77	1.30
1960	317.1	0.19	0.92	1.57
1970	333.9	0.22	1.04	1.92
1980	350.8	0.25	1.16	2.19
1990	366.9	0.28	1.28	2.44

[a]See details in section 3.1. Troposphere is defined as in Figure 2, based on the 150 ppbv "chemical tropopause." O_3, ozone, troposphere only; BC, black carbon; OC, organic carbon; $SO_4^=$, sulfate. Values are given in Tg.

burning causes significant increases throughout the Southern Hemisphere (+5–15 DU). The increased production of ozone within the troposphere causes the influx from the stratosphere to decrease slightly (from 365 to 345 Tg yr^{-1}). Present-day and preindustrial concentrations of ozone are evaluated with observations in sections 4.1–4.2, while recent trends in ozone are discussed in section 4.3.

[19] Aerosol concentrations rise more rapidly during the historical time period than ozone (Figure 2 and Table 3). The burden of sulfate increases by a factor of 3.6 from 1860 to 2000, with the largest increase occurring near the industrial source regions in the northern midlatitudes (Figure 4). Black carbon (Figure 5) and organic carbon (not shown) also increase considerably in regions of strong biofuel burning (East Asia and South Asia) and biomass burning (tropical Africa and South America), with the global burden increasing by a factor of 11.6 for BC and 6.1 for OC.

[20] A major uncertainty in the simulation of preindustrial concentrations of ozone and aerosols is the amount of historical biomass burning. The sensitivity of the simulated preindustrial concentrations to the assumptions about biomass burning was assessed using a sensitivity study. The standard simulation assumes that extratropical forest fire emissions in 1860 were the same as present-day emissions, while biomass burning emissions from all other sources were only 10% of present (section 2.3). In the sensitivity simulation, extratropical forest burning is also reduced to 10% of present. In this simulation, the global burden of tropospheric ozone in 1860 is reduced by 0.5 DU (5.5 Tg) versus the standard simulation, while the aerosol burdens are reduced by more than 30% for BC and 50% for OC. In the case of sulfate, for which biomass burning emissions of SO_2 are only a minor source, the burden in the sensitivity simulation changes little (<1%) from the standard case. The results of this biomass burning sensitivity simulation are discussed further in the context of the evaluation of preindustrial model results in section 4.2.

3.2. Future Results (2000–2100)

[21] In the future scenarios, the ozone trends (Figure 2 and Table 5) generally follow the projected NO_x emission trends (Figure 1). The largest increases in tropospheric ozone burden occur in the A1FI and A2 scenarios. In the A2 simulations, ozone increases from its year 2000 values by 13% (4.3 DU, or 46.6 Tg) in 2030, and by 42% (14.2 DU, or 155.0 Tg) in 2100. Ozone columns in the A2 scenario increase considerably by 2100 throughout the entire Northern Hemisphere and the tropical Atlantic Ocean, with maxima of >60 DU over South Asia, East Asia, the Middle East, North Africa, and the tropical South Atlantic (Figure 3). In contrast to the large increases in the A1FI and A2 scenarios, ozone in the A1B scenario increases modestly (12%) by 2100, while in the B1 scenario ozone increases by only 1.5 DU (16.7 Tg) through the mid-21st century and then decreases to 1.9 DU (20.9 Tg) below present-day values. The chemical production of tropospheric ozone increases from 5042 Tg yr^{-1} in 2000 to over 8600 Tg yr^{-1} in 2100 in A2 and A1FI and to over 6000 Tg yr^{-1} in A1B, while decreasing to 4548 Tg yr^{-1} in B1 (Table 6). The increase in tropospheric ozone predicted in this study for the A2 scenario in 2030 is within the range of 53 ± 10 Tg found in a 21-model ensemble for the A2 scenario in the PHOTOCOMP-2030 study [*Stevenson et al.*, 2006]. The increase by 2100 agrees well with the average value of ~15 DU from 10 CTMs in OxComp, corrected from the value reported in the IPCC-TAR [*Prather et al.*, 2001] (the reported value was 22 DU, but a note indicates that a processing error caused this value to be overstated). The OxComp study used a preliminary version of the A2 scenario, in which CH_4 concentrations were higher in 2100 (4300 ppbv) than in the final version of the scenario (3731 ppbv), tending to increase the tropospheric ozone column estimated for 2100 [*Prather et al.*, 2001].

[22] The future scenarios for aerosols differ considerably from those for ozone (Figure 2 and Table 5). In all four SRES scenarios considered, the sulfate aerosol burden (Figures 2 and 4) reaches its peak between 2020 and 2040 (13–46% above 2000 levels) and then declines sharply (to 4–45% below 2000 levels). Scenarios for black carbon (Figures 2 and 5) and organic carbon (Table 5) range from rapid increases throughout the period (reaching more than double their 2000 burden in the A1FI and A2 scenarios) to decreases after 2000 (decreasing by ~40% in the B1

Table 4. Global Budgets of Tropospheric Ozone From Historical and Present-Day Simulations[a]

Year	STE	Production	Loss	Dry Deposition
1860	365	2389	2306	450
1870	363	2581	2460	487
1880	363	2705	2558	512
1890	361	2816	2647	533
1900	360	2895	2712	547
1910	361	2998	2796	565
1920	359	3104	2885	581
1930	358	3221	2982	600
1940	358	3335	3076	620
1950	356	3498	3209	648
1960	354	3803	3460	700
1970	352	4202	3795	763
1980	349	4601	4129	825
1990	346	4951	4427	875

[a]See section 3.1. Troposphere is defined as extending from the surface to the hybrid model level at approximately 100 hPa in the tropics (30°S to 30°N) and 250 hPa in the extratropics. STE, stratosphere-troposphere exchange. Production, chemical production; loss, chemical loss. Values are given in Tg yr^{-1}.

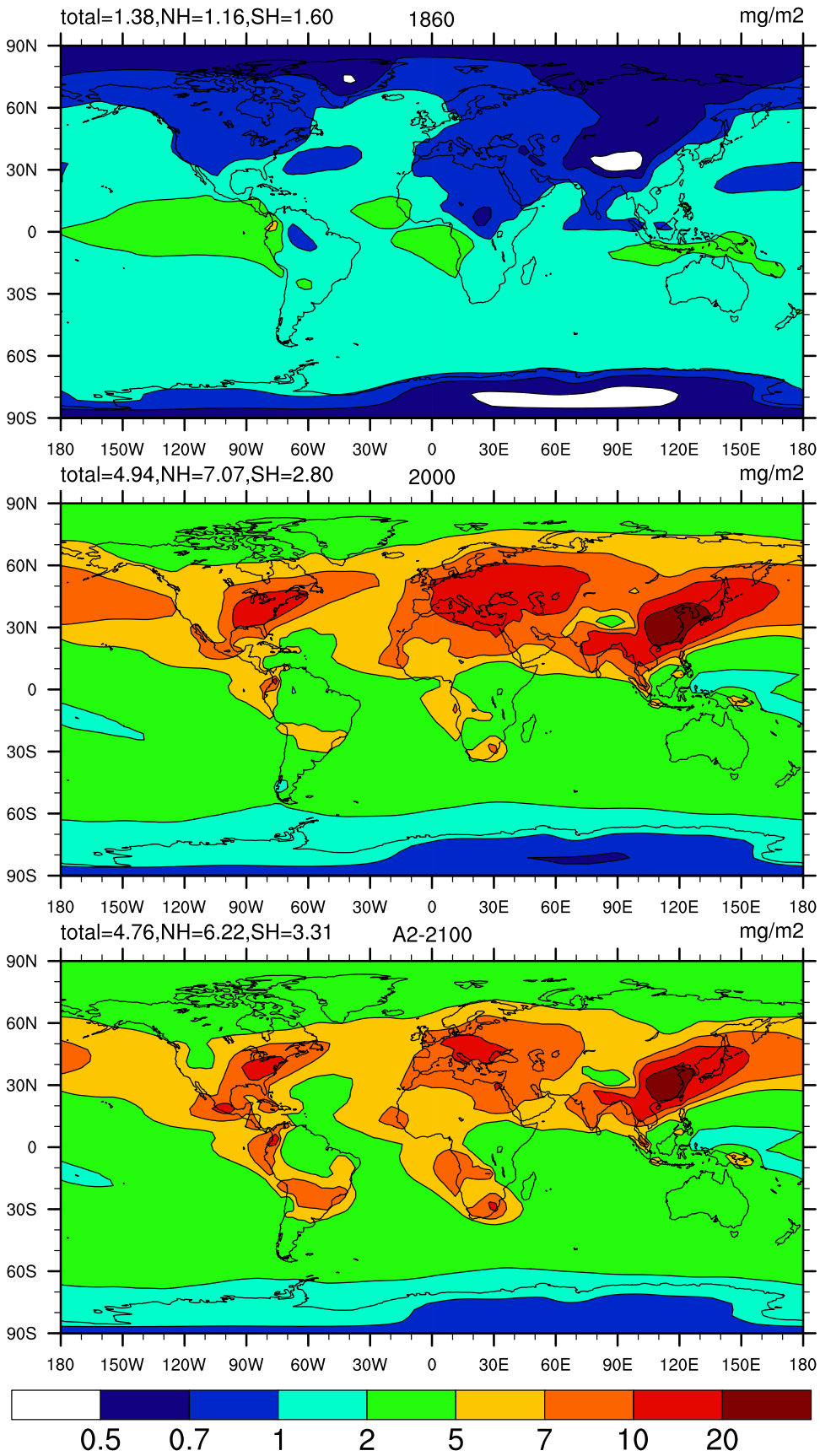

Figure 4. Total atmospheric column of sulfate aerosol (in mg $SO_4^{=}/m^2$) in simulations for (top) 1860 and (middle) 2000 and (bottom) the A2 scenario for 2100.

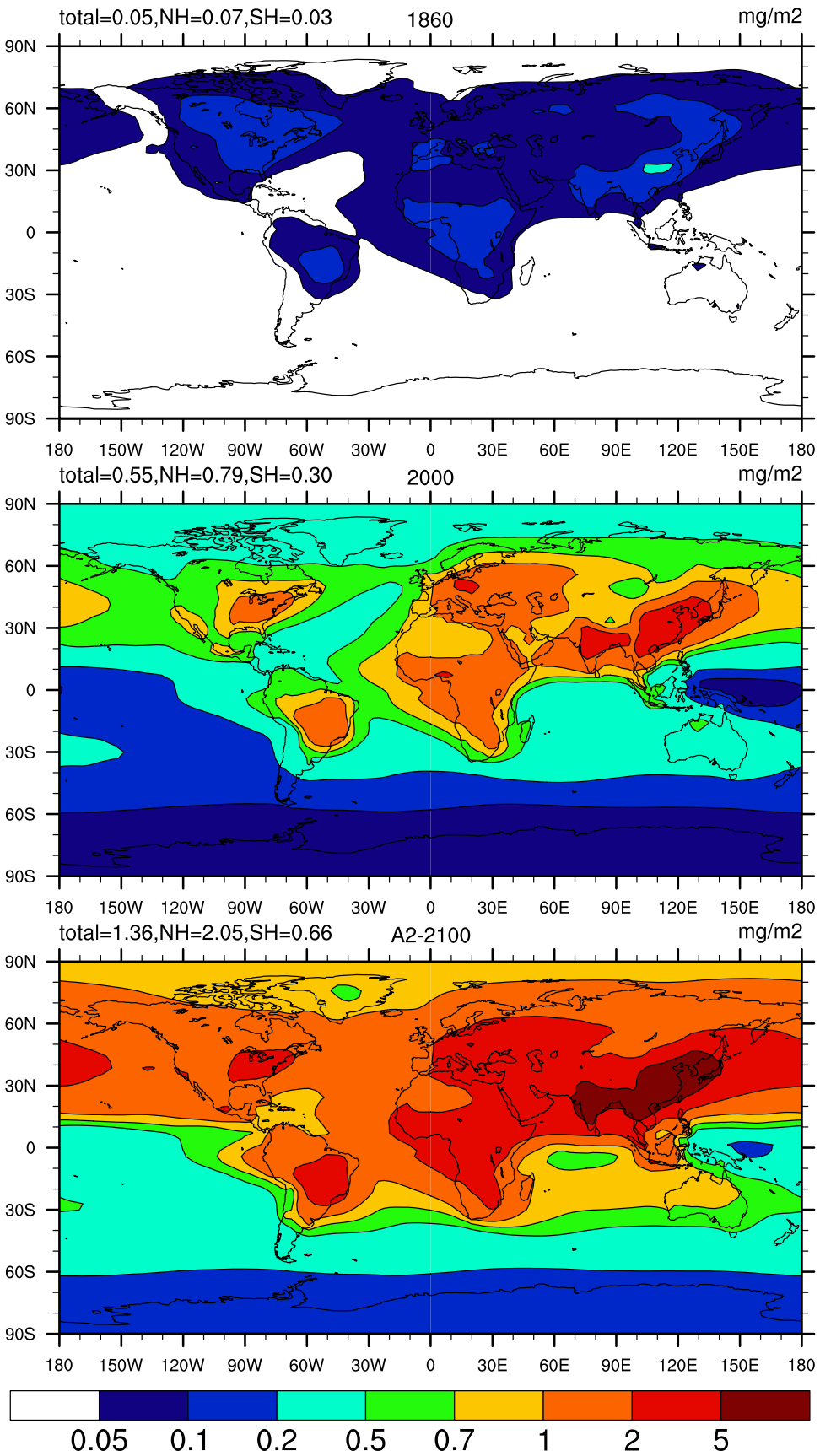

Figure 5. Total atmospheric column of black carbon aerosol (in mg C/m^2) in simulations for (top) 1860 and (middle) 2000 and (bottom) the A2 scenario for 2100.

Table 5. Global Burdens of Ozone, Black Carbon, Organic Carbon, and Sulfate From Future Scenario Simulations[a]

	A2				A1B				B1				A1FI			
Year	O_3	BC	OC	$SO_4^=$	O_3	BC	OC	$SO_4^=$	O_3	BC	OC	$SO_4^=$	O_3	BC	OC	$SO_4^=$
2000	372	0.28	1.28	2.52	372	0.28	1.28	2.52	372	0.28	1.28	2.52	372	0.28	1.28	2.52
2010	384	0.31	1.38	2.70	387	0.32	1.41	3.01	378	0.27	1.20	2.70	384	0.33	1.44	2.86
2020	400	0.34	1.48	3.34	403	0.33	1.43	3.38	385	0.26	1.16	2.74	403	0.39	1.64	3.03
2030	418	0.39	1.67	3.68	419	0.36	1.52	3.21	388	0.22	1.03	2.85	424	0.47	1.91	3.24
2040	431	0.41	1.76	3.61	425	0.37	1.57	2.65	388	0.21	0.97	2.86	449	0.56	2.23	3.21
2050	444	0.43	1.86	3.54	429	0.39	1.63	2.48	384	0.19	0.91	2.61	480	0.69	2.70	2.91
2060	457	0.47	1.98	3.17	430	0.40	1.66	2.04	379	0.19	0.90	2.25	501	0.72	2.80	2.31
2070	473	0.50	2.11	2.77	430	0.41	1.69	1.73	373	0.19	0.89	1.94	519	0.78	3.01	1.94
2080	490	0.55	2.29	2.54	425	0.43	1.77	1.59	367	0.18	0.87	1.71	536	0.84	3.28	1.86
2090	508	0.62	2.54	2.49	432	0.47	1.92	1.55	360	0.17	0.84	1.53	533	0.83	3.19	1.87
2100	527	0.69	2.79	2.43	417	0.51	2.08	1.50	351	0.16	0.81	1.39	530	0.79	3.06	1.87

[a]See section 3.2 for details. Troposphere is defined as in Figure 2, based on the 150 ppbv "chemical tropopause." O_3, ozone, troposphere only; BC, black carbon; OC, organic carbon; $SO_4^=$, sulfate. Values are given in Tg.

scenario), reflecting differences in projected emissions of these species (which are scaled to SRES CO emissions, see section 2.4).

4. Evaluation of Ozone Trends

4.1. Present-Day Concentrations

[23] Present-day ozone concentrations simulated by MOZART-2 have been evaluated extensively by H03 by comparison with vertical profiles and seasonal cycles from ozonesonde measurements (see Figures 3 and 4 in H03). Simulated ozone concentrations generally agree with the observed magnitude (within ±25%) and vertical gradient (Figure 6). At high northern latitudes (e.g., Resolute), and to a lesser extent some northern midlatitude stations (e.g., Hohenpeissenberg, Sapporo, and Wallops Island), the model tends to overestimate ozone near the tropopause by 25% or more, particularly in winter. This overestimate of ozone in the upper troposphere of the northern extratropics may result from inadequate resolution of the tropopause or excessive cross-tropopause transport of ozone. The spring or summer maximum of ozone in the lower and middle troposphere at northern midlatitudes, reflecting the seasonal cycle of photochemical ozone production (and possibly stratospheric influence) is well simulated (typically within one month). The magnitude and timing of the seasonal peak in the tropical lower troposphere (e.g., Ascension Island), which reflects the combined influences of biomass burning and dynamics, are also reproduced well by the model.

4.2. Preindustrial Concentrations

[24] Several sets of observations of surface ozone concentrations were made during the late nineteenth century. While most of these early observations were qualitative and suffered from significant interferences, the data sets have recently been reanalyzed and calibrated to reconstruct quantitative ozone concentrations [e.g., *Volz and Kley*, 1988; *Marenco et al.*, 1994; *Pavelin et al.*, 1999]. Many models of the preindustrial atmosphere have used these reconstructed data sets to evaluate the simulated preindustrial ozone concentrations [e.g., *Berntsen et al.*, 1997; *Wang and Jacob*, 1998; *Hauglustaine and Brasseur*, 2001; *Mickley et al.*, 2001; *Shindell et al.*, 2003; *Lamarque et al.*, 2005].

[25] The simulated 1880 ozone concentrations overestimate the preindustrial surface observations [*Volz and Kley*, 1988; *Pavelin et al.*, 1999] by 5–15 ppbv, and the observations at the high-altitude Pic du Midi site [*Marenco et al.*, 1994] by almost 20 ppbv. This overestimate is similar to that found by "standard" preindustrial simulations in other previous studies [*Wang and Jacob*, 1998; *Mickley et al.*, 2001; *Shindell et al.*, 2003; *Lamarque et al.*, 2005]. Sensitivity studies have shown that model simulations can be brought into better agreement with the preindustrial obser-

Table 6. Global Budgets of Tropospheric Ozone From Future Scenario Simulations[a]

	A2				A1B				B1				A1FI			
Year	STE	Prod.	Loss	Dry Dep.	STE	Prod.	Loss	Dry Dep.	STE	Prod.	Loss	Dry Dep.	STE	Prod.	Loss	Dry Dep.
2000	345	5042	4507	884	345	5042	4507	884	345	5042	4507	884	345	5042	4507	884
2010	342	5341	4762	926	341	5398	4809	934	343	5187	4630	905	343	5333	4755	925
2020	339	5719	5087	976	337	5757	5116	984	342	5353	4773	926	338	5766	5125	984
2030	335	6148	5457	1031	334	6105	5413	1031	341	5441	4851	936	333	6267	5558	1048
2040	332	6418	5691	1065	332	6210	5505	1043	342	5441	4854	934	328	6835	6050	1119
2050	329	6705	5940	1100	331	6301	5583	1055	342	5340	4767	920	321	7573	6690	1210
2060	327	7001	6195	1139	332	6317	5596	1059	344	5214	4662	901	318	8033	7088	1270
2070	324	7353	6499	1184	332	6313	5593	1059	344	5055	4527	877	315	8474	7467	1329
2080	321	7738	6832	1233	333	6211	5511	1039	346	4922	4413	860	311	8845	7791	1373
2090	317	8172	7208	1288	334	6117	5434	1023	347	4771	4283	840	313	8774	7728	1367
2100	312	8612	7591	1341	335	6039	5370	1010	350	4548	4099	803	313	8686	7649	1358

[a]See section 3.2. Troposphere is defined as extending from the surface to the hybrid model level at approximately 100 hPa in the tropics (30°S to 30°N) and 250 hPa in the extratropics. STE, stratosphere-troposphere exchange; prod., chemical production; loss, chemical loss; dep., dry deposition. Values are given in Tg yr^{-1}.

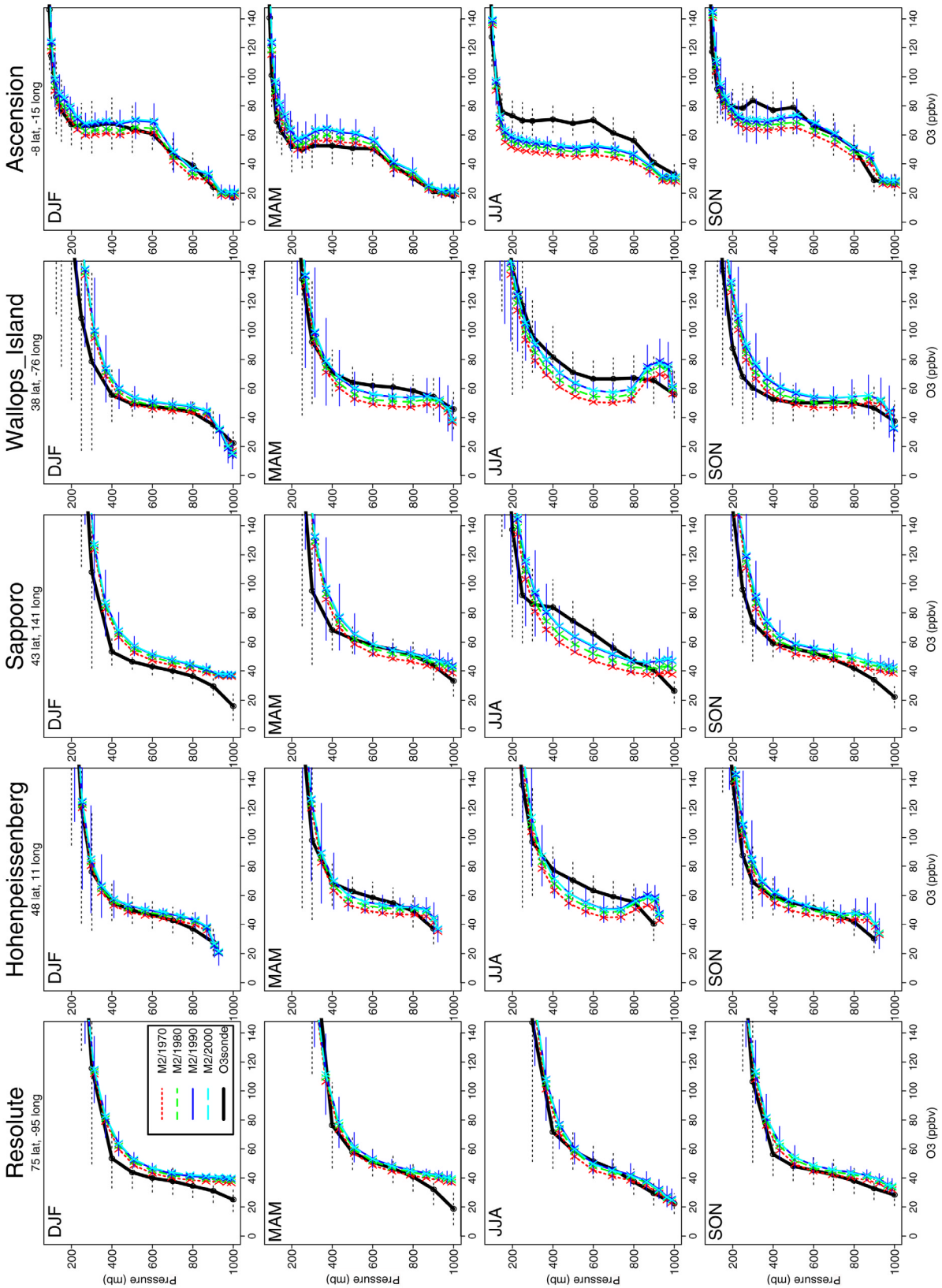

Figure 6. Comparison of observed (thick solid black lines) and simulated (thin lines in color, simulation years indicated in legend) seasonal vertical profiles of ozone volume mixing ratio (ppbv). Observations are from ozonesonde measurements compiled by *Logan* [1999]. Standard deviations of observed and simulated 1990 concentrations are indicated by horizontal bars.

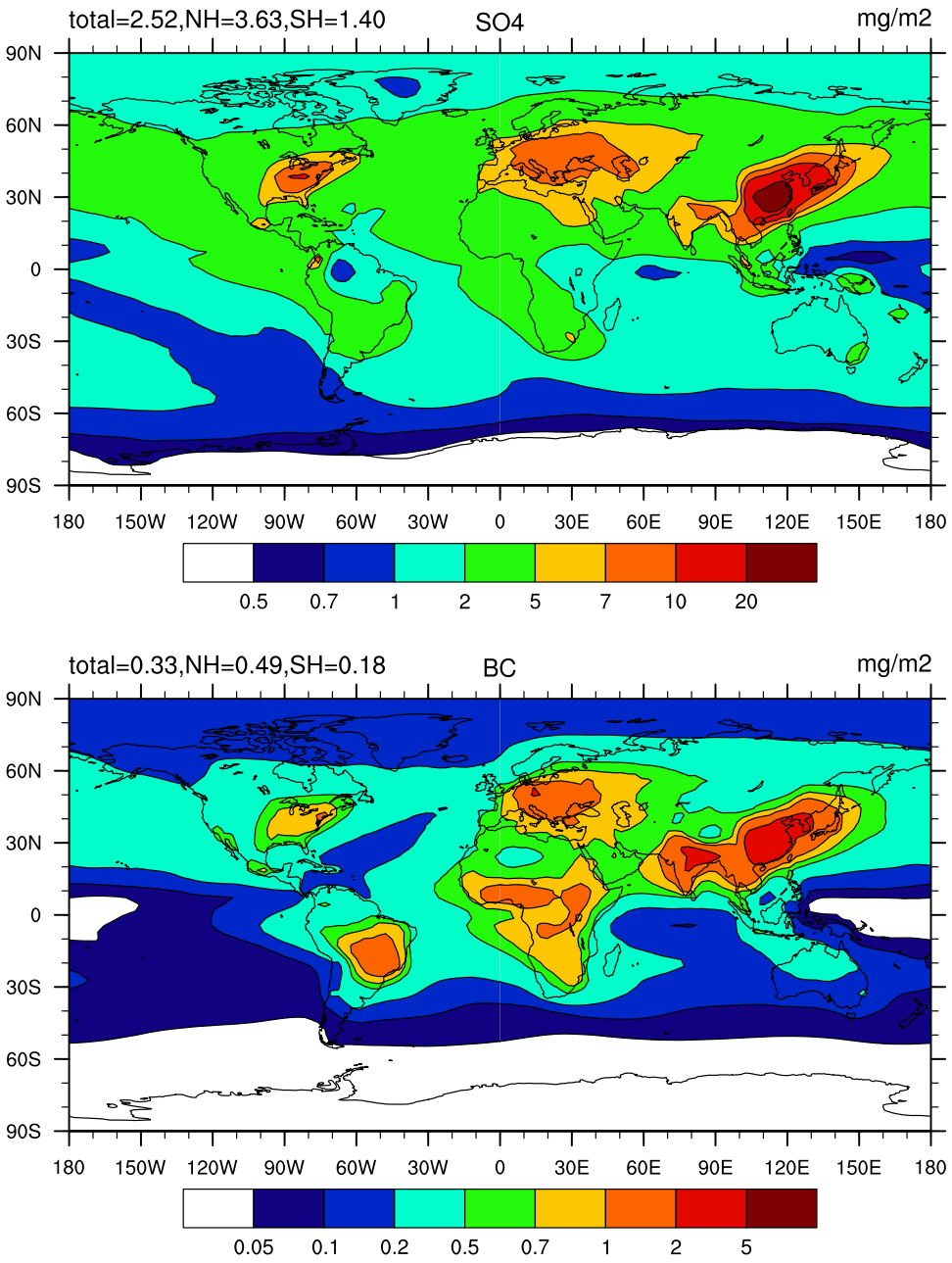

Figure 7. Total atmospheric column of (top) sulfate and (bottom) black carbon aerosol (in mg/m^2) in simulations for year 2000, with increased wet deposition rate (see section 5 for details). Compare with Figures 4 and 5 (middle panels), which show results of simulations with "standard" wet deposition rates.

vations by: decreasing the preindustrial sources of NO_x from lightning and soils [*Mickley et al.*, 2001; *Shindell et al.*, 2003], increasing biogenic hydrocarbon emissions [*Mickley et al.*, 2001; *Shindell et al.*, 2003], increasing dry deposition velocities [*Berntsen et al.*, 1997; *Hauglustaine and Brasseur*, 2001; *Lamarque et al.*, 2005], decreasing biomass burning emissions [*Hauglustaine and Brasseur*, 2001; *Lamarque et al.*, 2005], or decreasing anthropogenic emissions [*Lamarque et al.*, 2005] (assumed nonzero anthropogenic emissions in standard preindustrial simulation). In particular, *Mickley et al.* [2001] found that the changes needed to achieve agreement between their preindustrial simulation and observations would decrease the calculated ozone burden by 70–94 Tg (7.4–8.5 DU) versus their standard preindustrial simulation.

[26] If anthropogenic emissions are eliminated (i.e., considering the 1860 simulation instead of 1880), the annual mean surface ozone concentrations decrease by ~5 ppbv over Europe, Asia, and North America, with maximum decreases of ~10 ppbv over Europe during summer. The bias of the 1860 simulation versus the preindustrial observations is decreased by 2–5 ppbv compared with that in the 1880 simulation. Preindustrial ozone concentrations are also sensitive to the assumed biomass burning emissions. This

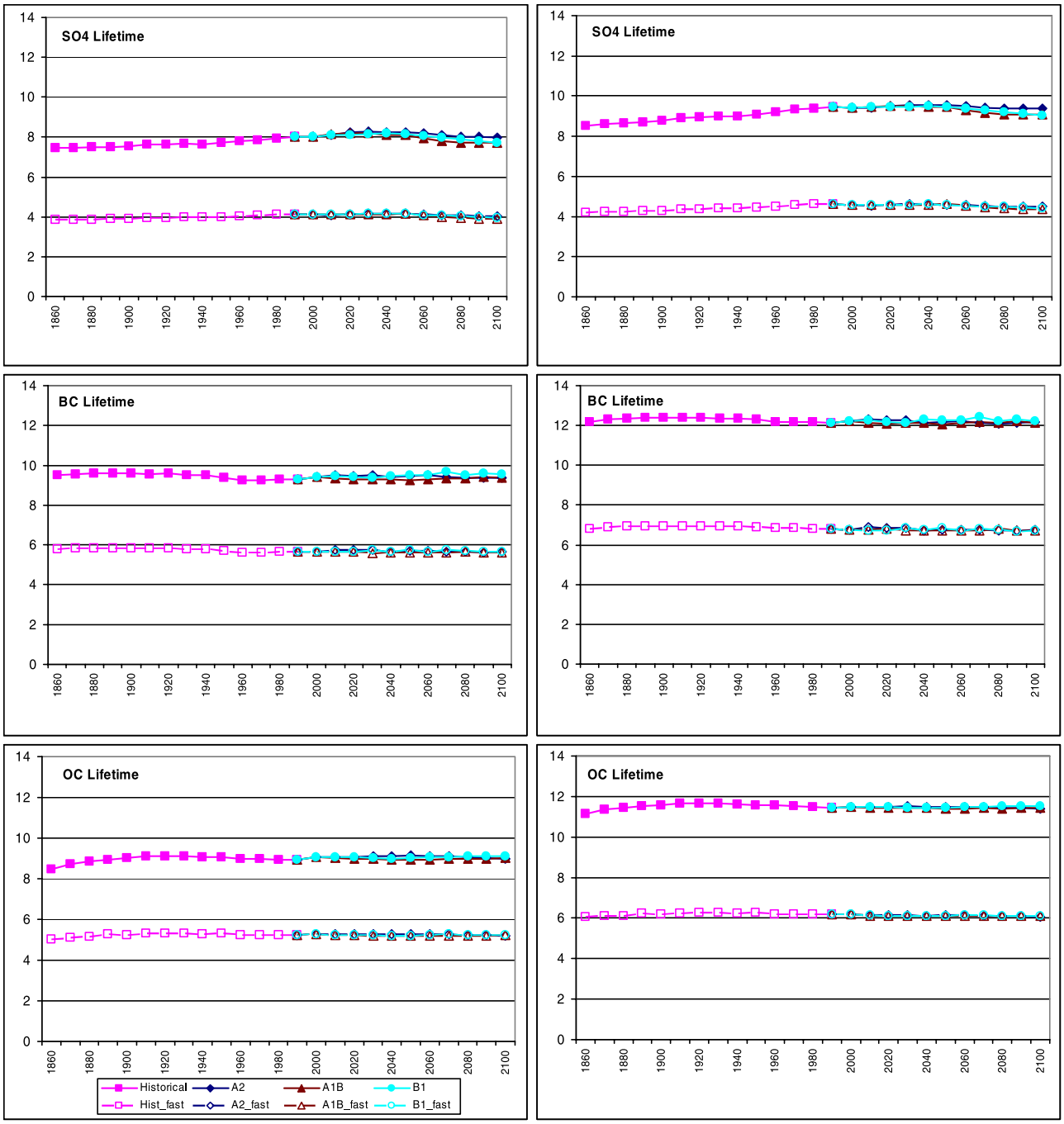

Figure 8. Simulated global average lifetimes (in days) of (top) sulfate ($SO_4^=$), (middle) black carbon (BC) and (bottom) organic carbon aerosol (OC) versus total removal (left panels) and wet deposition only (right panels) for 1860–2100. For the years 2010–2100, results are shown for simulations using emissions based on the IPCC-SRES scenarios A2, A1B, and B1. Solid symbols indicate lifetimes for simulations with standard wet deposition, and open symbols indicate sensitivity simulations with fast wet deposition (see section 5).

sensitivity is assessed here using the simulation for 1860 described in section 3.1, in which extratropical forest burning is decreased to 10% of present, rather than being held constant. In this sensitivity simulation, annual average surface ozone concentrations are reduced by 2–5 ppbv at northern midlatitudes (versus the standard 1860 simulation), further reducing the overestimate of preindustrial ozone observations to 6–12 ppbv for surface observations, and 13 ppbv at Pic du Midi.

4.3. Recent Trends

[27] Simulated tropospheric ozone concentrations increased from 1970 to 1990 at northern midlatitudes throughout the free troposphere, with the largest increases occurring

during the summer (Figure 6). These increases result from increased anthropogenic emission of NO_x and other ozone precursors during this period, primarily in Asia. Ozonesonde observations suggest that ozone increased over Europe and Japan during this period (by more than 20% in the free troposphere at Hohenpeissenberg and Sapporo), but decreased over Canada (>20% at Goose Bay) and showed little trend over the United States (Wallops Island) [e.g., *Logan*, 1994; *Logan et al.*, 1999]. Simulated concentrations (Figure 6) show an increase comparable to the observations at Hohenpeissenberg (10–15% throughout the year) and Sapporo (up to 25% in summer, 10–15% in other seasons), but show a small increase over Goose Bay (5–12%, not shown) and Wallops Island (10–15%), rather than the observed decrease or lack of trend. *Fusco and Logan* [2003] attribute some of the observed decrease over North America to a reduced input of ozone from the stratosphere, although even when this effect is included, their model still produces an increase in ozone over Goose Bay (1970–1995) in all seasons.

[28] Near-surface ozone concentrations in the model increase by 30–40% (approximately 10–20 ppbv) over Europe in summer during the period 1950–2000. The relative increase is much smaller than the factor of 2 increase estimated from observations by *Staehelin et al.* [2001], but the absolute change is similar to that observed. This discrepancy suggests that surface ozone concentrations may overestimate observations in 1950 by ~10 ppbv, similar to the model bias for preindustrial conditions (section 4.2).

5. Sensitivity to Aerosol Wet Removal

[29] Wet removal is the dominant sink for sulfate and carbonaceous aerosols. The parameterization of wet removal in models is highly uncertain and represents a large source of uncertainty in modeling aerosol species concentrations [e.g., *Cooke et al.*, 2002]. In order to test the dependence of the simulation results on the wet deposition parameterization, sensitivity runs were performed in which the wet deposition rates for sulfate and carbonaceous aerosols were doubled from their standard values (section 2.1). In these sensitivity simulations for the year 2000 (Figure 7), global aerosol burdens are decreased by ~50% for sulfate, and by ~40% for black carbon and organic carbon (not shown). The corresponding changes in the total lifetime and the lifetime versus wet deposition for each aerosol type are shown in Figure 8. The wet deposition lifetime for sulfate responds nearly linearly to the change in wet deposition rate, decreasing from a range of 8.5–9.6 days to 4.2–4.8 days. The sulfate burden correspondingly decreases by about 50%, since wet deposition is the dominant removal process for sulfate. The smallest decreases in surface concentrations are found near continental source regions (10–30% for sulfate), with the largest decreases over remote ocean regions (generally 30–60% for sulfate). The wet deposition lifetime of black and organic carbon aerosols respond less than linearly to the change in wet deposition rate, because a fraction of their emissions are in hydrophobic forms, which are unaffected by wet deposition until they are ''aged'' and converted into a hydrophilic forms (see sections 2.1–2.2). The presence of hydrophobic forms also causes the wet deposition lifetime for the carbonaceous aerosols to be larger than that for sulfate (~12 days versus ~9 days).

6. Conclusion

[30] Tropospheric ozone and aerosols are radiatively important trace species. Historical and projected future changes in their concentrations contribute significant (positive and negative) climate forcings [*Ramaswamy et al.*, 2001]. Because of their short lifetimes, the concentrations of ozone and aerosols are highly variable in space and time. In order to estimate the time-dependent 3-D distributions of these species, which are necessary for coupled climate model simulations, chemical transport models are typically used. In this study, estimated historical emissions and projected future emission scenarios are used to simulate the distributions of tropospheric ozone and aerosols throughout the period 1860–2100.

[31] Results presented here suggest that the chemical production rate of tropospheric ozone has increased by more than a factor of 2 since preindustrial times, resulting in a 50% increase in the tropospheric ozone burden, with an especially rapid increase since 1950. The largest increases occurred at northern middle to high latitudes as a result of anthropogenic emissions of ozone precursors. Ozone changes in the future vary considerably depending on the emissions scenario. In the most pessimistic scenarios (A2 and A1FI) ozone increases by over 40% from 2000 to 2100, while in the most optimistic scenario (B1) ozone decreases modestly (−6%) over the coming century. Historical changes in aerosol burdens are even larger than those for ozone. Sulfate aerosols are estimated to have increased by more than a factor of 3 versus preindustrial levels, while carbonaceous aerosols have increased by more than a factor of 6. Future scenarios also diverge considerably in their projected aerosol concentrations. For instance, all four scenarios produce initial increases in sulfate over the next several decades, but the net change from 2000 to 2100 ranges from −4% (A2) to −45% (B1).

[32] Comparisons with observations indicate several important uncertainties in this study. The preindustrial simulations overestimate surface ozone concentrations versus the few available measurements at that time. This suggests a possible error in the assumed magnitude of preindustrial emissions (e.g., biomass burning, biogenic emissions). This discrepancy can be reduced but not eliminated by using lower anthropogenic and biomass burning emissions than assumed in the 1880 simulation. If the preindustrial observations are accurate, the overestimate of ozone would imply an underestimate of the anthropogenic contribution to tropospheric ozone (and the associated radiative forcing), possibly by up to 10 DU (0.4 W m^{-2}) [*Mickley et al.*, 2001]. The simulation of present-day ozone generally matches observations well but tends to overestimate ozone in the upper troposphere at northern high and middle latitudes. If this overestimate is due to excessive stratosphere-troposphere exchange, it may be present throughout the simulation period. If instead it is due to excessive in situ production, the overestimate may be variable in time, increasing with increased precursor emissions.

[33] The simulated aerosol concentrations are shown to be highly sensitive to the rate of aerosol wet removal, which is poorly known. Doubling the aerosol wet deposition rates in a sensitivity simulation leads to a 50% decrease in the sulfate burden, and 40% decreases in carbonaceous aerosol burdens. This finding indicates a strong need for better algorithms for aerosol wet deposition in order to narrow the uncertainties in simulated aerosol burdens and the resulting radiative forcings.

[34] This study considers the effect of changes in anthropogenic emissions on the concentrations of tropospheric ozone and aerosols during the period 1860–2100. While emissions changes over this period are very large and are expected to dominate the change in ozone and aerosol concentrations, other concurrent changes also affect these concentrations. These changes, which are neglected in this study but have been considered separately in other studies, include: changes in stratospheric ozone, which affect stratosphere-to-troposphere exchange and photolysis rates [*Fusco and Logan*, 2003]; meteorological variability and trends, which affect water vapor concentrations, circulation and precipitation patterns, and production of NO_x from lightning [*Mickley et al.*, 2001; *Shindell et al.*, 2003; *Lamarque et al.*, 2005]; biogenic emissions changes (due to changes in land use, fertilizer application, temperature and precipitation) [*Mickley et al.*, 2001; *Shindell et al.*, 2003].

[35] Future anthropogenic emissions are highly uncertain. This study considered a range of four emission scenarios from SRES [*Nakićenović et al.*, 2000], widely used in climate models for the IPCC AR4 assessment and intended to span the range of possible future scenarios. More recent scenarios, such as those proposed by *Dentener et al.* [2005], suggest that if current emission control legislation targets are met (or exceeded), emissions of NO_x, CO, and NMVOCs could be significantly lower than assumed in the pessimistic SRES A2 scenario, and similar to (or lower than) those assumed in the more optimistic B1 scenario considered here.

[36] The simulated decadal concentrations of ozone and aerosols from this study have been employed in the GFDL coupled climate model simulations of historical and future climate, where they have been shown to substantially affect regional patterns of climate change [*Delworth et al.*, 2006; *Knutsen et al.*, 2006]. A companion paper extends the work done in this study by evaluating the aerosol distributions presented here and the resulting optical depths by comparison with observations [*Ginoux et al.*, 2006]. A future paper (V. Ramaswamy et al., manuscript in preparation, 2006) will discuss the direct radiative forcing produced in the climate model by these ozone and aerosol distributions.

[37] **Acknowledgments.** I would like to thank Arlene Fiore and Songmiao Fan for their useful comments on this manuscript and Xuexi Tie for providing the aerosol code he developed in MOZART. I would also like to thank Paul Ginoux and V. Ramaswamy for their helpful discussions about the work described here. Comments from two anonymous reviewers led to significant improvements in the manuscript and are greatly appreciated.

References

Andreae, M. O., and P. Merlet (2001), Emissions of trace gases and aerosols from biomass burning, *Global Biogeochem. Cycles*, *15*, 955–966.

Berntsen, T. K., I. S. A. Isaksen, G. Myhre, J. S. Fuglestvedt, F. Stordal, T. Alsvik Larsen, R. S. Freckleton, and K. P. Shine (1997), Effects of anthropogenic emissions on tropospheric ozone and its radiative forcing, *J. Geophys. Res.*, *102*, 28,101–28,126.

Brasseur, G. P., D. A. Hauglustaine, S. Walters, P. J. Rasch, J.-F. Müller, C. Granier, and X. X. Tie (1998), MOZART, a global chemical transport model for ozone and related chemical tracers: 1. Model description, *J. Geophys. Res.*, *103*, 28,265–28,289.

Cooke, W. F., C. Liousse, H. Cachier, and J. Feichter (1999), Construction of a $1° \times 1°$ fossil fuel emission dataset for carbonaceous aerosol and implementation and radiative impact in the ECHAM-4 model, *J. Geophys. Res.*, *104*, 22,137–22,162.

Cooke, W. F., V. Ramaswamy, and P. Kasibhatla (2002), A general circulation model study of the global carbonaceous aerosol distribution, *J. Geophys. Res.*, *107*(D16), 4279, doi:10.1029/2001JD001274.

Delworth, T. L., et al. (2006), GFDL's CM2 global coupled climate models. part 1: Formulation and simulation characteristics, *J. Clim.*, *19*, 643–674.

Dentener, F., D. Stevenson, J. Cofala, R. Mechler, M. Amann, P. Bergamaschi, F. Raes, and R. Derwent (2005), The impact of air pollutant and methane emission controls on tropospheric ozone and radiative forcing: CTM calculation for the period 1990–2030, *Atmos. Chem. Phys.*, *5*, 1731–1755.

Dentener, F., et al. (2006), The global atmospheric environment for the next generation, *Environ. Sci. Technol.*, *40*, 3586–3594.

Friedl, R. (Ed.) (1997), Atmospheric effects of subsonic aircraft: Interim assessment report of the advanced subsonic technology program, *NASA Ref. Publ., 1400*, 143 pp.

Fusco, A. C., and J. A. Logan (2003), Analysis of 1970–1995 trends in tropospheric ozone at Northern Hemisphere midlatitudes with the GEOS-CHEM model, *J. Geophys. Res.*, *108*(D15), 4449, doi:10.1029/2002JD002742.

Gauss, M., et al. (2003), Radiative forcing in the 21st century due to ozone changes in the troposphere and the lower stratosphere, *J. Geophys. Res.*, *108*(D9), 4292, doi:10.1029/2002JD002624.

Ginoux, P., M. Chin, I. Tegen, J. M. Prospero, B. Holben, O. Dubovik, and S.-J. Lin (2001), Sources and distributions of dust aerosols simulated with the GOCART model, *J. Geophys. Res.*, *106*, 20,255–20,273.

Ginoux, P., L. W. Horowitz, V. Ramaswamy, I. V. Geogdzhayev, B. N. Holben, G. Stenchikov, and X. Tie (2006), Evaluation of aerosol distribution and optical depth in the GFDL coupled model CM2.1 for present climate, *J. Geophys. Res.*, *111*, D22210, doi:10.1029/2005JD006707.

Giorgi, F., and W. L. Chameides (1985), The rainout parameterization in a photochemical model, *J. Geophys. Res.*, *90*, 7872–7880.

Grenfell, J. L., D. T. Shindell, D. Koch, and D. Rind (2001), Chemistry-climate interactions in the Goddard Institute for Space Studies general circulation model: 2. New insights into modeling the preindustrial atmosphere, *J. Geophys. Res.*, *106*, 33,435–33,452.

Guenther, A., et al. (1995), A global model of natural volatile organic carbon emissions, *J. Geophys. Res.*, *100*, 8873–8892.

Hack, J. J. (1994), Parameterization of moist convection in the NCAR community climate model (CCM2), *J. Geophys. Res.*, *99*, 5551–5568.

Hao, W. M., and M.-H. Liu (1994), Spatial and temporal distribution of tropical biomass burning, *Global Biogeochem. Cycles*, *8*, 495–503.

Hauglustaine, D. A., and G. P. Brasseur (2001), Evolution of tropospheric ozone under anthropogenic activities and associated radiative forcing of climate, *J. Geophys. Res.*, *106*, 32,337–32,360.

Haywood, J., and O. Boucher (2000), Estimates of the direct and indirect radiative forcing due to tropospheric aerosols: A review, *Rev. Geophys.*, *38*(4), 513–543.

Henderson, S. C., and U. K. Wickrama (1999), Aircraft emissions: Current inventories and future scenarios, in *Aviation and the Global Atmosphere*, edited by J. E. Penner et al., chap. 9, pp. 291–331, Cambridge Univ. Press, New York.

Hess, P. G., S. Flocke, J.-F. Lamarque, M. C. Barth, and S. Madronich (2000), Episodic modeling of the chemical structure of the troposphere as revealed duing the spring MLOPEX 2 intensive, *J. Geophys. Res.*, *105*, 26,809–26,839.

Holtslag, A., and B. Boville (1993), Local versus nonlocal boundary-layer diffusion in a global climate model, *J. Clim.*, *6*, 1825–1842.

Horowitz, L. W., et al. (2003), A global simulation of tropospheric ozone and related tracers: Description and evaluation of MOZART, version 2, *J. Geophys. Res.*, *108*(D24), 4784, doi:10.1029/2002JD002853.

Kiehl, J. T., J. J. Hack, G. B. Bonan, B. A. Boville, D. L. Williamson, and P. J. Rasch (1998), The National Center for Atmospheric Research Community Climate Model: CCM3, *J. Clim.*, *11*, 1131–1149.

Knutsen, T. R., T. L. Delworth, K. W. Dixon, I. M. Held, J. Lu, V. Ramaswamy, M. D. Schwarzkopf, G. Stenchikov, and R. J. Stouffer (2006), Assessment of twentieth-century regional surface temperature trends using the GFDL CM2 coupled models, *J. Clim.*, *19*, 1624–1651.

Lamarque, J.-F., P. Hess, L. Emmons, L. Buja, W. Washington, and C.Granier (2005), Tropospheric ozone evolution between 1890 and 1990, *J. Geophys. Res.*, *110*, D08304, doi:10.1029/2004JD005537.

Levy, H., II, P. S. Kasibhatla, W. J. Moxim, A. A. Klonecki, A. I. Hirsh, S. J. Oltmans, and W. L. Chameides (1997), The global impact of human activity on tropospheric ozone, *Geophys. Res. Lett.*, *24*, 791–794.

Lin, S.-J., and R. B. Rood (1996), Multidimensional flux-form semi-Lagrangian transport schemes, *Mon. Weather Rev.*, *124*, 2046–2070.

Logan, J. A. (1994), Trends in the vertical distribution of ozone: An analysis of ozonesonde data, *J. Geophys. Res.*, *99*, 25,553–25,585.

Logan, J. A. (1999), An analysis of ozonesonde data for the troposphere: Recommendations for testing 3-D models and development of a gridded climatology for tropospheric ozone, *J. Geophys. Res.*, *104*, 16,115–16,149.

Logan, J. A., et al. (1999), Trends in the vertical distribution of ozone: A comparison of two analyses of ozonesonde data, *J. Geophys. Res.*, *104*, 26,373–26,400.

Madronich, S., and S. Flocke (1998), The role of solar radiation in atmospheric chemistry, in *Handbook of Environmental Chemistry*, edited by P. Boule pp. 1–26, Springer, New York.

Marenco, A., H. Gouget, P. Nédélec, J.-P. Pagés, and F. Karcher (1994), Evidence of a long-term increase in tropospheric ozone from Pic du Midi data series: Consequences: Positive radiative forcing, *J. Geophys. Res.*, *99*, 16,617–16,632.

Mauzerall, D. L., and X. P. Wang (2001), Protecting agricultural crops from the effects of tropospheric ozone exposure: Reconciling science and standard setting in the United States, Europe, and Asia, *Annu. Rev. Energy Environ.*, *26*, 237–268.

Mickley, L. J., P. P. Murti, D. J. Jacob, J. A. Logan, D. M. Koch, and D. Rind (1999), Radiative forcing from tropospheric ozone calculated with a unified chemistry-climate model, *J. Geophys. Res.*, *104*, 30,153–30,172.

Mickley, L. J., D. J. Jacob, and D. Rind (2001), Uncertainty in preindustrial abundance of tropospheric ozone: Implications for radiative forcing calculations, *J. Geophys. Res.*, *106*, 3389–3400.

Müller, J.-F. (1992), Geographical distribution and seasonal variation of surface emissions and deposition velocities of atmospheric trace gases, *J. Geophys. Res.*, *97*, 3787–3804.

Nakićenović, N., et al. (2000). *Emissions Scenarios: A Special Report of Working Group III of the Intergovernmental Panel on Climate Change*, 599 pp., Cambridge Univ. Press, New York.

Olivier, J. G. J., A. F. Bouwman, C. W. M. van der Maas, J. J. M. Berdowski, C.Veldt, J. P. J. Bloos, A. J. H. Visschedijk, P. Y. J. Zandveld, and J. L. Haverlag (1996), Description of EDGAR version 2.0: A set of global emission inventories of greenhouse gases and ozone-depleting substances for all anthropogenic and most natural sources on a per country basis and on a 1×1 degree grid, *RIVM Rep. 771060 002/TNO-MEP Rep. R96/119*, Natl. Inst. for Public Health and the Environ., Bilthoven, Netherlands.

Pavelin, E. G., C. E. Johnson, S. Rughooputh, and R. Toumi (1999), Evaluation of preindustrial surface ozone measurements made using Schönbein's method, *Atmos. Environ.*, *33*, 919–929.

Penner, J. E., et al. (2001), Aerosols, their direct and indirect effects, in *Climate Change 2001: The Scientific Basis, Contribution of Working Group I to the Third Assessment Report of the Intergovernmental Panel on Climate Change*, edited by J. T. Houghton et al., chap. 5, pp. 289–348, Cambridge Univ. Press, New York.

Prather, M., et al. (2001), Atmospheric chemistry and greenhouse gases, in *Climate Change 2001: The Scientific Basis, Contribution of Working Group I to the Third Assessment Report of the Intergovernmental Panel on Climate Change*, edited by J. T. Houghton et al., chap. 4, pp. 239–287, Cambridge Univ. Press, New York.

Price, C., J. Penner, and M. Prather (1997), NO_x from lightning: 1. Global distribution based on lightning physics, *J. Geophys. Res.*, *102*, 5929–5941.

Ramaswamy, V., et al. (2001), Radiative forcing of climate change, in *Climate Change 2001: The Scientific Basis, Contribution of Working Group I to the Third Assessment Report of the Intergovernmental Panel on Climate Change*, edited by J. T. Houghton et al., chap. 6, pp. 349–416, Cambridge Univ. Press, New York.

Rasch, P. J., N. M. Mahowald, and B. E. Eaton (1997), Representations of transport, convection, and the hydrologic cycle in chemical transport models: Implications for the modeling of short-lived and soluble species, *J. Geophys. Res.*, *102*, 28,127–28,138.

Shindell, D. T., G. Faluvegi, and N. Bell (2003), Preindustrial-to-present-day radiative forcing by tropospheric ozone from improved simulations with the GISS chemistry-climate GCM, *Atmos. Chem. Phys.*, *3*, 1675–1702.

Staehelin, J., N. R. P. Harris, C. Appenzeller, and J. Eberhard (2001), Ozone trends: A review, *Rev. Geophys.*, *39*(2), 231–290.

Stevenson, D. S., et al. (2006), Multi-model ensemble simulations of present-day and near-future tropospheric ozone, *J. Geophys. Res.*, *111*, D08301, doi:10.1029/2005JD006338.

Tie, X., S. Madronich, S. Walters, D. P. Edwards, P. Ginoux, N. Mahowald, R. Zhang, C. Lou, and G. Brasseur (2005), Assessment of the global impact of aerosols on tropospheric oxidants, *J. Geophys. Res.*, *110*, D03204, doi:10.1029/2004JD005359.

van Aardenne, J. A., F. J. Dentener, G. J. Olivier, C. G. M. Klein Goldewijk, and J. Lelieveld (2001), A $1^\circ \times 1^\circ$ resolution data set of historical anthropogenic trace gas emissions for the period 1890–1990, *Global Biogeochem. Cycles*, *15*, 909–928.

Volz, A., and D. Kley (1988), Evaluation of the Montsouris series of ozone measurements made in the nineteenth century, *Nature*, *332*, 240–242.

Wang, Y., and D. J. Jacob (1998), Anthropogenic forcing on tropospheric ozone and OH since preindustrial times, *J. Geophys. Res.*, *103*, 31,123–31,135.

Wesely, M. L. (1989), Parameterization of surface resistance to gaseous dry deposition in regional-scale numerical models, *Atmos. Environ.*, *23*, 1293–1304.

World Health Organization (WHO) (2003), Health aspects of air pollution with particulate matter, ozone and nitrogen dioxide, report on a WHO working group, Bonn, Germany.

Yienger, J. J., and H. Levy II (1995), Empirical model of global soil-biogenic NO_x emissions, *J. Geophys. Res.*, *100*, 11,447–11,464.

Zender, C. S., H. Bian, and D. Newman (2003), Mineral Dust Entrainment and Deposition (DEAD) model: Description and 1990s dust climatology, *J. Geophys. Res.*, *108*(D14), 4416, doi:10.1029/2002JD002775.

Zhang, G. J., and N. A. McFarlane (1995), Sensitivity of climate simulations to the parameterization of cumulus convection in the Canadian Climate Centre general circulation model, *Atmos. Ocean*, *33*, 407–446.

L. W. Horowitz, NOAA Geophysical Fluid Dynamics Laboratory, 201 Forrestal Road, Princeton, NJ 08540, USA. (larry.horowitz@noaa.gov)